Electr Eng
DOI 10.1007/s00202-016-0458-2

ORIGINAL PAPER

Nickel–titanium shape memory alloy-actuated thermal overload relay system design

S. Dilibal[1] · **H. Sahin**[1] · **E. Dursun**[2] · **E. D. Engeberg**[3]

Received: 1 June 2016 / Accepted: 4 October 2016

Abstract Nickel–titanium (NiTi) shape memory alloy (SMA) actuated electromechanical applications are becoming widespread in many mechatronics systems. In the thermal overload electromechanical relays (EMRs), the bimetallic strips which provide one-dimensional linear motion are used for activation. In this study, the actuation of the thermal overload EMR system is provided using the NiTi SMAs with novel EMR designs instead of traditional bimetallic strips. Two different nickel–titanium shape memory alloy-actuated thermal overload relays are designed to provide thermal overload protection for varied mechatronics systems. The displacement parameter of the designs is extracted from the established constitutive model for the NiTi SMA-actuated thermal overload relay. The developed antagonistic design structures provide functionality which is convenient for the thermal overload relays. Additionally, the developed NiTi SMA-actuated thermal overload relay designs can function in varied electrical current ranges compared to the traditional bimetallic EMRs which need to be produced separately for different electrical current ranges.

Keywords NiTi shape memory alloy · Thermal overload relay · Solid-state relay · Electromechanical relay

✉ S. Dilibal
savas.dilibal@gedik.edu.tr

[1] Mechatronics Engineering Department, Istanbul Gedik University, 34876 Yakacık Kartal, Istanbul, Turkey

[2] Department of Electrical and Electronics Engineering, Marmara University, 34722 Goztepe, Istanbul, Turkey

[3] Ocean and Mechanical Engineering Department, Florida Atlantic University, 777 Glades Road, Boca Raton, FL 33431, USA

1 Introduction

NiTi shape memory alloys (SMAs) have become potential actuator candidates for many lightweight and compact mechatronics [1], adaptive [2] and adaptronic systems [3]. SMA-based electromechanical systems typically operate under a large number of thermomechanical cycles [4] under different mechanical and thermal loadings. NiTi SMAs are a unique class of intermetallic material which can recover as large as 8 % strain associated with the shape memory effect behavior in the range of the operating temperatures [5]. The thermomechanical response of the NiTi SMA can be stabilized using the thermomechanical processing techniques, which affect directly the shape memory properties of the NiTi SMA. Due to their high strength-to-weight ratio [6], NiTi SMAs have found many applications in electromechanical devices such as energy harvesters [7–9], pumps [10], bioinspired octopuses [11], robotic fingers [12–14], and prosthetic hands [15]. In addition to these applications, the NiTi SMA-actuated thermal overload relay system will be a novel candidate for next generation relays.

Electromechanical bimetallic thermal overload relays are preferred in a range of different applications; such as power system [16,17], automation [18] and aerospace protective devices [19]. These types of relays can uniquely control high current electrical circuit systems due to their ability to conduct high electrical currents. In contrast to solid-state transistor technologies which reduce the size of the switching system by using semiconductor materials, the electromechanical thermal overload relays are indispensable for high current power systems.

In addition to the high current strength, the EMRs do not need any heat sink compared to the SSR counterparts. The SSRs are developed by the integration of the

Published online: 19 October 2016

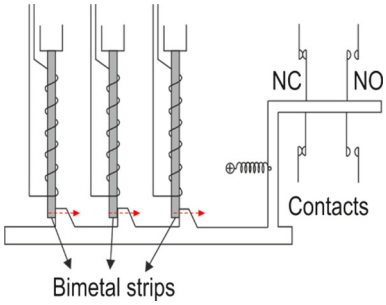

Fig. 1 The schematic of the conventional thermal overload protection relay

solid-state technology into the electrical and electronics engineering applications. The SSRs are discovered to obtain high bandwidth frequency response in mechatronics systems. However, the maintenance of the SSRs is not sustainable due to the electrical current leakage in the circuit and impulsive voltage drops across to the circuits. On the other hand, there is a total line-to-load cut off when the contacts of EMRs are open. The EMRs can switch any AC or DC power in a short time. Additionally, they operate at full load over a wide temperature range [19]. Although the usage of SSRs is becoming widespread, the necessity for the EMRs continues especially for the protection of high current electrical motors, such as in spacecraft applications [20].

The thermal overload EMRs are designed to cut power if the motor draws too much current for an extended period of time. When excessive current flows through the motor circuit, the relay opens due to increased motor temperature, relay temperature, or sensed overload current depending on the relay type. Thermal overload relays are designed to control the motor's heating profile [21]. Hence, the overload must occur for an extended period before the circuit is interrupted. Bimetallic strips which are placed in the thermal overload EMRs consist of two metals that have different thermal expansion coefficients. Bimetallic strips tend to bend over the metal which has lower thermal expansion when Joule heated. The thermal overload relays activate when the placed bimetallic strips are heated through the flow of current in an electrical circuit. Upon overloading, the bimetallic strips bend and make normally open contacts as shown in Fig. 1. Cold or hot roll bonding process is widely used for the production of bimetallic strips, such as Al/Cu, Cu/Ag, Al/Ni, etc., [22]. The obtained mechanical displacement is used in a range of different mechatronics devices, such as thermostats, thermometers, circuit breakers and electromechanical relays.

NiTi SMAs exhibits two fascinating characteristics which are called superelasticity and shape memory effect. They exhibit these characteristics with the phase transformation between martensite and austenite states. The microstructural phase transformation which occurs through the formation of the martensitic crystallographic structure from the high temperature phase (austenite) causes the stress-induced superelastic or thermal-induced shape memory effect responses in the macrostructure. While the superelastic response occurs through the loading/unloading, the shape memory effect occurs through the heating/cooling cycles. Hence, the stress-induced martensitic transformation (SIMT) produces the superelasticty while thermal-induced martensitic transformation (TIMT) generates the shape memory effect (Fig. 2). The shape memory effect can be divided into two different subsystems. One is one-way shape memory effect (OWSME), the other is two-way shape memory effect (TWSME). The material composition, heat treatments, precipitations, shape memory training process affect the response of the NiTi SMAs. The electrical resistivity of the NiTi SMA varies as a function of temperature through the crystallographic transformation between martensite and austenite. Figure 3 shows the electrical resistance vs temperature response of the NiTi SMA wire. The obtained two curves in Fig. 3 represent the change in resistance upon heating above the austenite finish temperature and cooling below the martensite finish temperature. The resistance–temperature curve shows a slight increase and a sharp drop during heating. During the cooling path, the resistance–temperature curve shows a steep increase until reaching the martensitic phase temperature [23].

The material response can be represented using constitutive equations for the mechanical behavior of the NiTi SMA such as stress, strain and temperature through the energy equations. In this study, the constitutive equation which can also be used for control applications is configured to represent the mechanical behavior of the NiTi SMA. The SMA modeling approaches can be classified in three different modeling approaches of micro- [24], meso- [25] and macroscale [26]. Each modeling technique has its own theoretical background as seen in Fig. 4. The multiscale modeling which consists of the combination of micro-, meso- and macro-scale modeling techniques using convenient theories can extract more realistic results than the constrained counterparts [27].

The thermomechanical behavior of SMAs can be modeled in various methods which are summarized in reference [28]. The continuum theory is used to establish a constitutive model for the SMA response. One degree of freedom constitutive models for NiTi SMA to realize the thermomechanical response are described as a polynomial, exponential, trigonometric or Fremond models in the literature. The polynomial models are more convenient to apply control theories compared to the other constitutive models. The simplicity of the polynomial model makes it useful for control applications [29,30].

In the present work, two novel NiTi SMA-actuated antagonistic designs are proposed for a functional thermal overload EMR system which can be utilized between 0.2 and 80 Amp

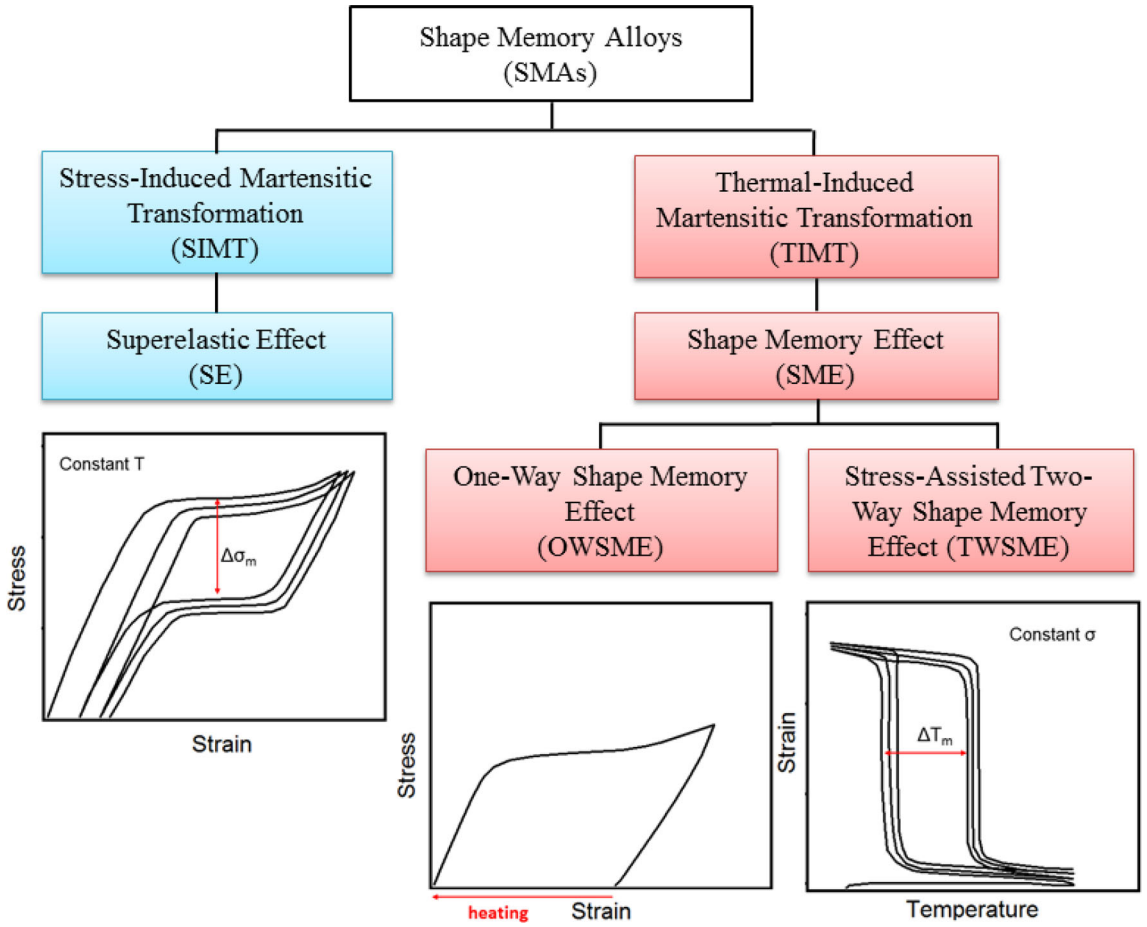

Fig. 2 A schematic for the thermomechanical responses of shape memory alloys

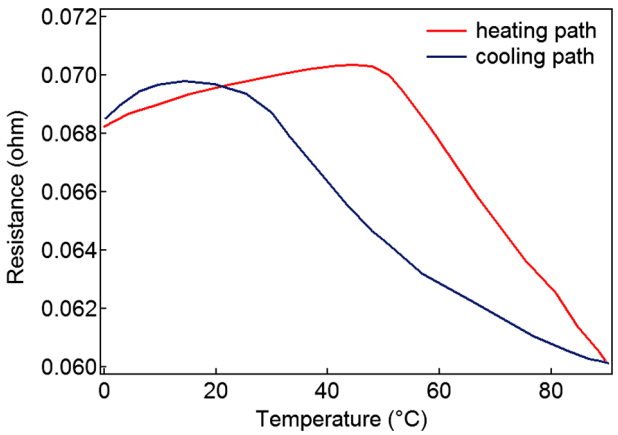

Fig. 3 The resistance vs temperature response of the NiTi SMA wire [18]

current ranges. A constitutive model is built for the thermal overload EMR switches which are used for receiving the displacement and temperature data. The SMA constitutive model performed by Zhao [27] is modified to be used for this specific relay application.

2 Materials characterization and model parameters

The materials characterization and the parametric investigation were carried out on the polycrystalline NiTi SMA wire with a 1.5 mm diameter. Perkin-Elmer Instruments Pyris-1 differential scanning calorimetry (DSC) is utilized to determine the forward and reverse phase transformation temperatures. The DSC analysis is conducted with the 15 °C per minute heating and cooling rate. The stress-free DSC analysis results give the martensitic and austenitic phase transformation peaks which provide the operation temperature range for the NiTi SMA samples. The martensitic transformation cycle consists of the following temperatures which are martensite finish temperature (M_f), martensite start temperature (M_s) austenite start temperature (A_s) and austenite finish temperature (A_f). The overheating of the NiTi SMAs causes the loss of the memorized shape due to the heat treatment. Figure 5 shows the DSC analysis result of the 1.5 mm NiTi SMA wire during the stress-free thermal cycling. The DSC results for the phase transformation characteristic temperatures indicated the following values of the martensite finish

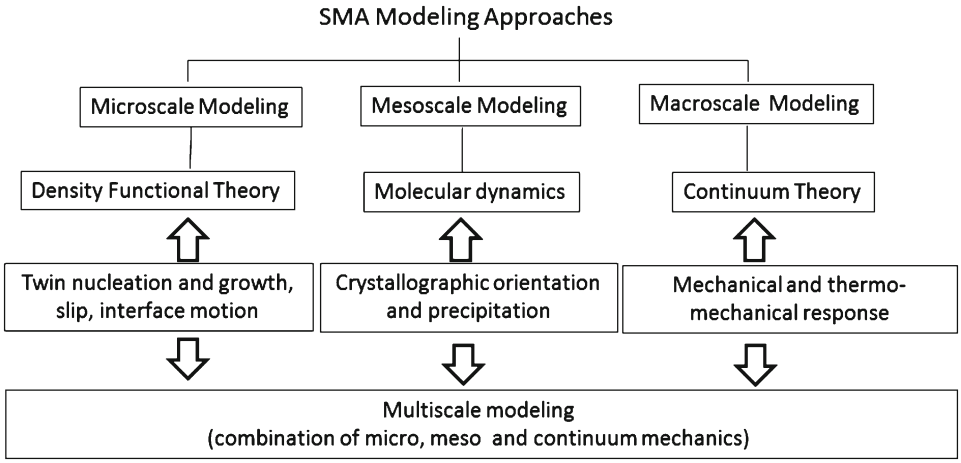

Fig. 4 A schematic for SMA modeling approaches

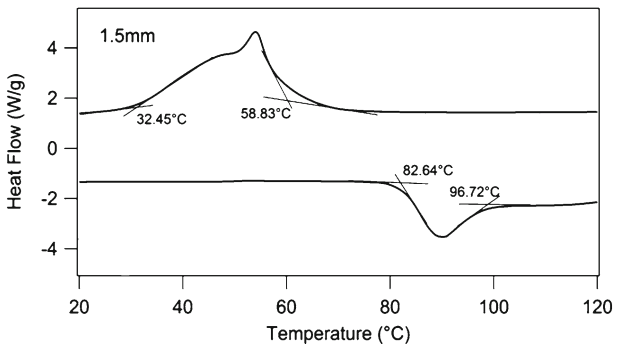

Fig. 5 DSC analysis result of the 1.5 mm NiTi SMA wire

(M_f) temperature = 32.45 °C, martensite start (M_s) temperature = 58.83 °C, austenite start (A_s) temperature = 82.64 °C, and austenite finish (A_f) = 96.72 °C. These phase transformation temperature results are used as model parameters.

The values of heat constant (C_p), Young modulus in martensitic (E_M) and austenitic phase (E_A) are received from reference [27]. The detailed model parameters with values of the NiTi SMA are depicted in Table 1. In addition, the nomenclatures of the NiTi SMA-actuated thermal overload relay are shown in Table 2.

3 The established NiTi SMA-actuated relay model

The macro-, meso-, or micro-scale SMA system modeling approaches can be selected depending on the established mechatronics system requirements as seen in Fig. 4. Each modeling approach has its own benefits and constraints. To receive the temperature–strain response which unveils the displacement data, a macro-scale model with continuum theory is established for the NiTi SMA-actuated relay system. The heating and cooling cycles of the relay system are simulated based on the shape memory characteristic of the NiTi SMAs. The established model is constructed in MatLab/Simulink software package in order to obtain the time–temperature and time–displacement plots.

The flowchart of the summarized model is described in Fig. 6. The model flowchart consists of six different modules which are referred to as SMA relay controller, heat transfer, phase transformation, kinematics, dynamics and constitutive model for the SMA relay. The constitutive model for SMA relay is the main module of the model which is integrated with the rest of the modules to receive or transmit the parametric results. The SMA relay controller module receives the temperature feedback from the heat transfer module while sending the temperature data to the heat transfer module. The heat transfer module sends temperature and temperature rate data to both phase transformation and constitutive model for the SMA relay modules. The phase transformation module receives the stress and stress rate from the constitutive model for the SMA relay module while sending the martensite fraction rate to the constitutive model for the SMA relay module. The kinematics module receives the displacement rate from the dynamics module while sending the strain rate to the constitutive model for the SMA relay. The dynamics module receives the stress values from the constitutive model for the relay SMA module while sending the displacement and displacement rate values.

The heat transfer model receives the voltage as an input while sending temperature and differential of the temperature as an output as seen in Eq. (1). In Eq. (1), m_w is the mass per unit length.

$$m_w c_p \dot{T} = \frac{V^2}{R} - hA_w (T - T_{amb}) \quad (1)$$

Phase transformation equations are as in the Eqs. (2)–(7) [17]. The inputs to this module are temperature, rate of change for the temperature and rate of change for stress.

The cooling transformation is defined as in the Eqs. of the (2) to (4).

Table 1 Model parameters with values for the NiTi SMA

Symbol	Parameter	Value	Symbol	Parameter	Value
C_p	Heat constant	320 J/kg °C	E_M	Young modulus (martensite)	40 Gpa
h_0	First heat convection factor	20	E_A	Young modulus (austenite)	75 Gpa
h_2	Second heat convection factor	0.001	l_o	Wire initial length	60 mm

Table 2 Nomenclatures of the NiTi SMA-actuated thermal overload relay

Symbol	Parameter	Symbol	Parameter
C_p	Heat constant	E_M	Young modulus (martensite)
h_0	First heat convection factor	E_A	Young modulus (austenite)
h_2	Second heat convection factor	l_o	Wire initial length
Ω	Phase transformation constant	Θ	Thermal expansion coefficient
M_s	Martensite start temperature	M_f	Martensite finish temperature
A_s	Austenite start temperature	A_f	Austenite finish temperature
ξ_M	The initial martensite fraction	ξ_A	The initial austenite fraction
C_M	Material coefficient for martensite fraction	C_A	Material coefficient for austenite fraction
V	The applied voltage	A_w	Wire surface area
T_{amp}	The ambient temperature	R	Resistance per unit length

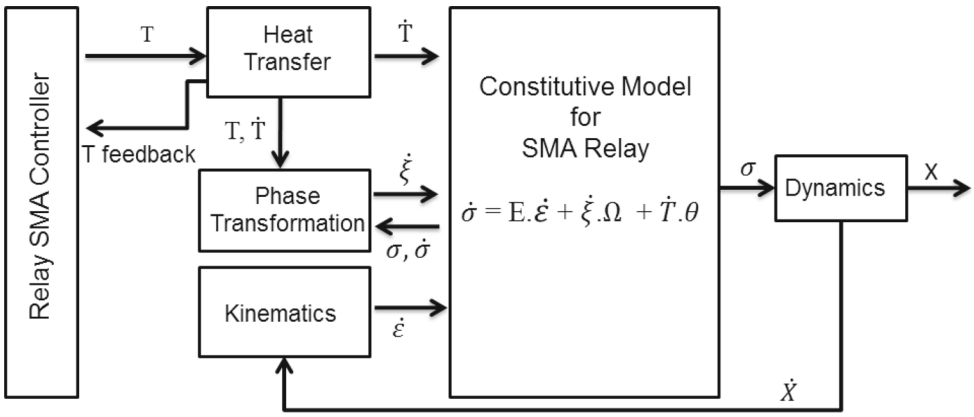

Fig. 6 The flowchart for the constitutive model of the NiTi SMA

$$\left(\dot{T} - \frac{\dot{\sigma}}{C_M}\right) < 0 \tag{2}$$

$$\dot{\xi} = \left(\frac{1-\xi_A}{2}\right).(\sin[a_M.(T - M_f) + b_M.\sigma]).\left(a_M.\dot{T} + b_M.\dot{\sigma}\right) \tag{3}$$

$$M_s + \frac{\sigma}{C_M} \le T \le M_f + \frac{\sigma}{C_M} \tag{4}$$

The heating transformation is defined as in the Equations of the (5) to (7).

$$\left(\dot{T} - \frac{\dot{\sigma}}{C_M}\right) > 0 \tag{5}$$

$$\dot{\xi} = \left(\frac{-\xi_M}{2}\right)(\sin[a_A.(T - A_s) + b_A.\sigma]).\left(a_A.\dot{T} + b_A.\dot{\sigma}\right) \tag{6}$$

$$A_s + \frac{\sigma}{C_A} \le T \le A_f + \frac{\sigma}{C_A} \tag{7}$$

The applied force on the NiTi SMA wire is calculated using the result of stress and cross-sectional area as in the Eq. (8).

F as in the Equation of the (8) is the input to the system of Eq. (9).

$$F = \sigma \cdot A_w \tag{8}$$

Dynamic response of the system determined using the dynamic equation of motion as seen in the Eq. (9).

$$F = M.\ddot{x} + B.\dot{x} + K.x \tag{9}$$

Constitutive model uses the Eq. (10).

$$\dot{\sigma} = E\dot{\varepsilon} + \Omega\,\dot{\xi} + \Theta\,\dot{T} \tag{10}$$

The phase transformation equation is shown in the Eq. (11).

$$\Omega = -\varepsilon_L E \tag{11}$$

If the thermal expansion part is neglected, the constitutive equation becomes as in the Eq. (12).

$$\dot{\sigma} = E\dot{\varepsilon} - \varepsilon_L E\dot{\xi} \tag{12}$$

The output of this model is the stress value" σ".

The kinematic model has elongation rate ($\dot{x}$) as input and strain rate as an output which is shown by Eq. (13).

$$\dot{\epsilon} = \frac{\dot{x}}{l} \tag{13}$$

The modulus of elasticity is calculated using Eq. (14).

$$E = \xi E_M + (1 - \xi) E_A \tag{14}$$

Here, the input signal to this equation is the stress value as described by Eq. (15).

$$\sigma = \int_0^t E\left(\dot{\epsilon} - \epsilon_L \dot{\xi}\right) dt + \sigma_0 \tag{15}$$

Finally, the force is calculated using Eq. (16).

$$F = A\sigma = k\varepsilon l \tag{16}$$

The stiffness for the force equation is derived using Equation (17).

$$k = \frac{A\sigma}{\epsilon l} \tag{17}$$

The parameter "k" varies with the value of the stress as seen in the Eq. (17). However, the "k" values for the martensite and austenite phases can be defined as constant equations (18).

$$k_M = \frac{E_M A}{l}, \quad k_A = \frac{E_A A}{l} \tag{18}$$

4 Model results

The time–temperature and time–displacement results are received from the model for the design purpose. The time–temperature result which is depicted in Fig. 7, shows that the NiTi SMA wire with 1.5 mm diameter warms up from 25 °C up to 100 °C in a maximum of 2 s. However, the cooling segment takes more than 20 s as shown in Fig. 7. As

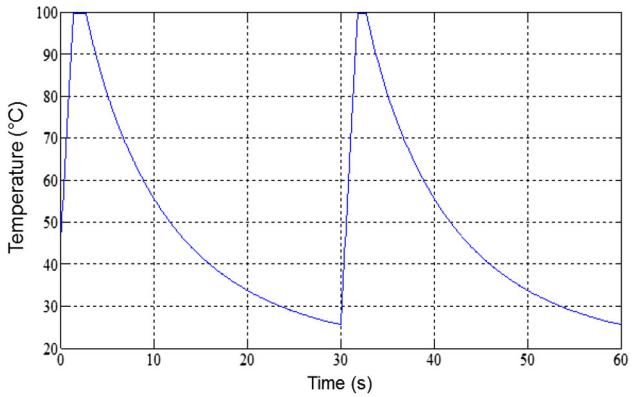

Fig. 7 Temperature vs time plots obtained from model result for the NiTi SMA wire with 1.5 mm diameter

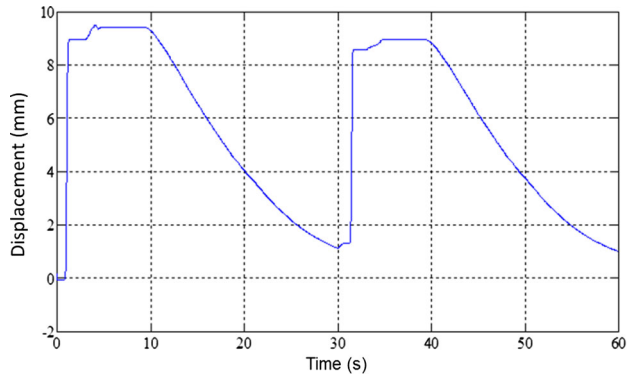

Fig. 8 Displacement vs time plots obtained from model result for the NiTi SMA wire with 1.5 mm diameter

determined from DSC analysis, the martensitic phase transformation starts at 58.8 °C for this specific material. The maximum displacement can be reached while the wire is heated above the austenite start temperature. The heat rate and temperature control can be varied under a large amount of heating cycles of the motor. The reference temperature is changed in between 25 °C to 100 °C every 30 s to realize one-cycle of displacement. Additionally, the algebraic loop for the simulated model is avoided with a convenient filter. The voltage is used as an input for the temperature reference input as seen in the result and in the Eq. (1). The displacement result matches with the temperature result as shown in Fig. 8.

5 The designs of the thermal overload relay

The CAD models of different designs of antagonistically actuated NiTi SMA thermal overload EMR are built for comparison purposes. Two novel designs are shown in Figs. 9, 10 in which the NiTi SMA wires are drawn in blue and red color to demonstrate their cold and hot states, respectively.

The first design is constructed on the rod which transmits the translational motion to the angular motion as shown in Fig. 9a. In this design, the bias spring and NiTi SMA wires work antagonistically to transmit the motion. When the overcurrent flows through the NiTi SMA wire, it heats up quickly to austenite final temperature where the wire contracts. In this phase, the NiTi SMA wire applies the pulling force on the rod which will open the relay switch as shown in Fig. 9b. Upon cooling of the wire, the NiTi SMA wire reverses back to the original length which causes the contact of the relay switch to close.

The second antagonistically actuated NiTi SMA relay design is constructed on the pulley system which rotates to transmit the angular motion to the translational motion as seen in Fig. 10a. The antagonistic design of the NiTi SMA wire and bias spring functions on the pulley system as seen in the design. The overcurrent flow causes the NiTi SMA wire to heat up. When the temperature of the NiTi SMA wire approaches the austenite final temperature, it contracts. This contraction causes the pulling force on the pulley system which opens the contact of the relay as shown in Fig. 10b. Upon cooling of the NiTi SMA wire, it reverses back to the original length which causes to close the contact of the relay switch.

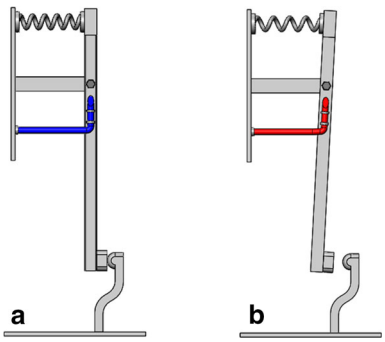

Fig. 9 Antagonistically actuated NiTi SMA thermal overload relay design with a lever

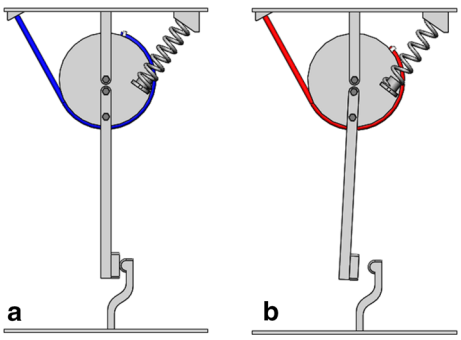

Fig. 10 Antagonistically actuated NiTi SMA thermal overload relay design with a pulley

6 Conclusion

The work presented emphasizes two different designs of functional NiTi SMA-actuated thermal overload relay systems for the thermal protection of several mechatronics applications. The novel NiTi SMA-actuated thermal overload protection relay systems provide significant advantage over the traditional bimetallic EMRs or SSRs. One specific NiTi SMA-actuated thermal overload relay can function in varied electrical current ranges compared to the bimetallic EMRs or SSRs which have to be manufactured separately for different electrical current ranges. Hence, the NiTi SMA-actuated thermal overload relays can be used as an alternative protective device to prevent thermal overload for the mechatronics control systems. The established model provides the temperature and displacement data for the NiTi SMA-actuated relays. The model results show that the developed designs are applicable for establishing a state-of-the-art SMA-actuated relay prototypes to conduct in the experimental stage. One such novel application would be for adaptronics and smart robotic systems that function both as an actuator and a current overload protector. In a future study, the NiTi SMA-actuated relay prototypes will be built and their performance analyses will be studied.

References

1. Elahinia M, Shayesteh Moghaddam N, Taheri Andani M, Amerinatanzi A, Bimber B.A, Hamilton R.F (2016) Fabrication of NiTi through additive manufacturing: a review. Progress in Materials Science
2. Leng J, Yan X, Zhang X, Huang D, Gao Z (2016) Design of a novel flexible shape memory alloy actuator with multilayer tubular structure for easy integration into a confined space. Smart Mater Struct 25:2
3. Schneider D, Lauer M, Voigt I, Drossel WG (2016) Development and examination of switchable heat pipes. Appl Thermal Eng 99:857–865
4. Hartl D, Lagoudas CD (2007) Aerospace applications of shape memory alloys. J Aerosp Eng 221(4):535–552
5. Dilibal S (2013) Investigation of nucleation and growth of detwinning mechanism in martensitic single crystal NiTi using digital image correlation. Metallogr Microstruct Anal 2:242–248
6. Nespoli A, Besseghini S, Pittaccio S, Villa E, Viscuso S (2010) The high potential of shape memory alloys in developing miniature mechanical devices: a review on shape memory alloy mini-actuators. Sensor Actuat A-Phys 158:149–160
7. Browne A, Johnson N, Wittorf M (2012) Energy harvesting, storing, and conversion utilizing shape memory activation, patent US 8.104.278 B2
8. Sreekumar M, Nagarajan T, Singaperumal M, Zoppi M, Molfino R (2007) Critical review of current trends in shape memory alloy actuators for intelligent robots. Indus Robot 34:285–294
9. Hegana A, Hariharan SI, Engeberg E (2016) Electromechanical conversion of low temperature waste heat via helical shape memory alloy actuators. IEEE/ASME Trans Mechatron 21:1434–1444
10. Pierce M, Mascaro S (2013) A biologically inspired wet shape memory alloy actuated robotic pump. IEEE/ASME Trans Mechatron 18:536–546

11. Mazzolai B, Margheri L, Cianchetti M, Dario P, Laschi C (2012) Soft-robotic arm inspired by the octopus: II. from artificial requirements to innovative technological solutions. Bioinspiration & Biomimetics
12. Engeberg E, Dilibal S, Vatani M, Choi J, Lavery J (2015) Anthropomorphic finger antagonistically actuated by SMA plates. Bioinspiration & Biomimetics
13. Dilibal S., Engeberg E.D. (2015) Finger-like manipulator driven by antagonistic NiTi shape memory alloy actuators, IEEE Int. Conference on Advanced Robotics, Istanbul
14. Silva A, Santos A, Souto C, Araujo C, Silva S (2013) Artificial biometric finger driven by shape-memory alloy wires. Artif Organs 37:965–972
15. Andrianesis K, Tzes A (2014) Development and control of a multifunctional prosthetic hand with shape memory alloy actuators. J Intell Robot Syst 78:257–289
16. Lu Y, Chung JL (2013) Detecting and solving the coordination curve intersection problem of overcurrent relays in subtransmission systems with a new method. Electric Power Syst Res J 95:19–27
17. Elmitwally A, Gouda E, Eladawy S (2015) Optimal allocation of fault current limiters for sustaining overcurrent relays coordination in a power system with distributed generation. Alex Univ Eng J 54:1077–1089
18. http://www.teledynerelays.com/hi-rel.asp, accessed 15 May 2016
19. Mahaffey TR (2002) Electromechanical relays versus solid-state: each has its place. Electronic Design 50:19
20. Mengshoel OJ, Darwichse A, Cascio K, Chavira M, Poll S, Uckun S (2008) Diagnosing faults in electrical power systems of spacecraft and aircraft, IAAI'08 Proceedings of the 20th national conference on Innovative applications of artificial intelligence, 31699-1705
21. Venkataraman B, Godsey B, Premerlani W, Shulman E, Thakur M, Midence R (2005) Fundamentals of a motor thermal model and its applications in motor protection. In: Pulp and Paper Industry Technical Conference
22. Khosravifard A, Ebrahimi R (2010) Investigation of parameters affecting interface strength in Al/Cu clad bimetal rod extrusion process 31–1:493–499
23. Kyriakides E, Hadjistassou C, Georgiou J (2012) A new memristor based on NiTi smart alloys, IEEE International Symposium on Circuits and Systems, 1403–1406
24. Liangliang G, Yong L, Teng YN (2014) An investigation on the crystal structure of $Ti_{50}Ni_{50-x}Cu_x$ shape memory alloys based on density functional theory calculations. Intermatalics 53:20–25
25. Bhattacharya K (2003) Microstructure of martensite. Oxford Series on Materials Modeling, Oxford
26. Mohamed B (2010) Mathematical modeling and control of nonlinear oscillators with shape memory alloys. Dissertation, Wilfrid Laurier University
27. Guoa Z, Pana Y, Weeb LB, Yu H (2015) Design and control of a novel compliant differential shape memory alloy actuator. Sens Actuator A-Phys 225:71–80
28. Piccirillo V, Goes LCS, Balthazar JM (2009) A shape memory alloy oscillator: regular and chaotic behavior, using basin of attractions approach. In: Proceedings of COBEM 2009
29. Paiva A, Savi MA (2006) An overview of constitutive models for shape memory alloys. Mathematical problems in engineering 1–30
30. Ashish K, Vidyashankar B (2009) Models for shape memory alloy behavior: an overview of modeling approaches. Int J Struct Changes Solids Mech Appl 1:111–148